Supplementary materials

1. Methods

1.1. Resveratrol (R) loaded nanoparticle formulae Optimization. To optimize the formulae of nanoparticles, total soy PC weight was considered as 7 mg and the ratio of other compounds, including αTA, Kolliphor® HS15, and R, were compared to PC, to determine the optimal composition for reaching high levels of physical stability, encapsulation efficiency, loading capacity and ΔDCN cells binding affinity *in vitro* and *in vivo*. DSPE-PEG_{5000} and DSPE-PEG_{5000}-peptide were used to replace 5 mol% of PC to synthesize Rnano and L-Rnano. Characteristics, encapsulation efficiency, physically stability and binding efficiency of nanoparticles were determined as main manuscript described.

1.2. Nanoparticles physical stability. To determine the stability of nanoparticles at different temperatures, freshly prepared Rnano and L-Rnano were aliquoted into black tubes and stored at 4°C, 22°C, and 37°C for 3 days. The particle size and PI were measured using a Brookhaven BI-MAS particle size analyzer, and the zeta potential was measured using a Zeta PALS analyzer every 24 hours.

1.3. *In vivo* fluorescence intensity. The mice were sacrificed to separate the BAT, I-WAT, G-WAT, RP-WAT and liver for *ex vivo* imaging to determine the biodistribution pattern of DiD-loaded Rnano and L-Rnano using an IVIS in vivo imaging system. Then, the DiD intensity was analyzed using the NIH image J software.

1.4. ASC targeting specificity of nanoparticles in RP-WAT. After IVIS imaging, RP-WAT was enzymatically digested and SVF was collected, washed, lysed, counted and resuspended in flow buffer at 1×10^7 cells/mL. SVF cells were stained with fluorophore-conjugated antibodies and analyzed using the Attune NxT flow cytometer as main manuscript described.

1.5. Measure the weight of RP-WAT and I-BAT. After sacrifice, brain, liver, lung, spleen, kidneys, skeletal muscle, BAT, RP-WAT, I-WAT and G-WAT of each mouse were collected, and weighed.

1.6. Tissue weight of G-WAT and I-WAT. After sacrifice, G-WAT and I-WAT were collected, weighted and imaged.

1.7. I-WAT and G-WAT mRNA expression. Total RNA was extracted from I-WAT and G-WAT using a TRIzol® reagent and cDNA was synthesized from quantified RNA using a Maxima First Strand cDNA Synthesis Kit according to the manufacturer's instructions. cDNA levels of target genes were measured using PowerUp SYBR™ green master mix on a real-time PCR system (Eppendorf Mastercycler® ep realplex instrument, NY). The mRNA-fold changes were calculated using the $2^{-\Delta\Delta Ct}$ method, which were normalized against the

housekeeping gene 36B4. Primer sequences of target genes are listed in **Table S3**.

1.8. Measurement of plasma inflammatory cytokines. Plasma concentrations of cytokines and chemokine (TNF-α, MCP-1, IL-6, IFN-γ) were measured using the bead-based LEGENDplex™ mouse inflammation panel kit and analyzed on the Attune NxT flow cytometer. The data were analyzed using the LEGENDplex™ analysis software.

1.9. Safety evaluation. Five mice from each group were randomly selected for safety evaluation as main manuscript described.

2. Results

2.1. Optimization of nanoparticle formulae

The particle size, PI, encapsulation efficiency, physical stability, binding affinity to ΔDCN cells and nanoparticle target and accumulation in WAT in C57BL/6J mice were used to optimize and screen nanoparticle formulae.

First, in order to increase R's encapsulation efficiency in nanoparticles, we fixed the PC weight and proportionally increased the weight of αTA, Kolliphor® HS15, and R to synthesize Rnano (**Table S1**). As the R loading amount increased, R precipitated out of Rnano and accumulated at the bottom of the tube after storing them at 37°C for 24 hours. Therefore, the optimal weight ratios of PC: R were 7:4 and 7:5, which do not have R precipitation.

Second, to further optimize the formulae, Rnano stability and R's encapsulation efficiency were measured. As the weight of αTA and Kolliphor® HS15 was increased, R's encapsulation efficiency increased, while the mean diameters of Rnano decreased. The physical stability of Rnano prepared using different formulae were compared (**Fig. S1A**). As the weight ratios of αTA and Kolliphor® HS15 to PC increased, the physical stability of Rnano increased. For example, when comparing low αTA and Kolliphor® HS15 content (PC: αTA: Kolliphor® HS15: R = 7:20:20:4, weight ratio) to high αTA and Kolliphor® HS15 content (PC: αTA: Kolliphor® HS15: R = 7:22:22:4, weight ratio), the mean diameters of Rnano increased 20 nm or less than 5 nm over 5 days at 37°C at low and high αTA and Kolliphor® HS15 content, respectively. Hence, high αTA and Kolliphor® HS15 content formulae were chosen.

After selecting the range of ratios of PC: αTA: Kolliphor® HS15: R from 7:22:22:4 to 7:34:34:5, the binding affinity of Rhoda-labeled L-Rnano to ΔDCN cells was further used to optimize formulae. As the ratios of PC to αTA and Kolliphor® HS15 were changed from 7:32:32 to 7:34:34 with the same R loading amount, the binding affinity to and uptake of Rhoda-L-Rnano by ΔDCN cells were decreased (**Fig. S1B**). Therefore, two formulae finalists (PC: αTA: Kolliphor® HS15: R = 7:22:22:4 and 7:32:32:5) were selected for a final testing in C57BL/6J mice.

Finally, WAT accumulation of DiD-labeled L-Rnano in C57BL/6J mice were used to select the final formula. After 24 hours of post-injection of DiD-labeled Rnano and L-Rnano, mice and the isolated BAT, RP-WAT, GWAT, I-WAT, and liver were visualized using the IVIS system. The higher DiD fluorescence intensity (blue color) indicated more nanoparticle accumulation. Under both finalist formulae, L-Rnano compared to Rnano had a higher accumulation in WAT *in situ* (**Fig. S1C**), and in isolated I-WAT and G-WAT, and lower accumulation in the liver (**Fig. S1D**). In addition, DiD-labeled L-Rnano made of formula 7:22:22:4 compared to 7:32:32:5 had much higher fluorescence signals in WAT, especially

I-WAT. Therefore, we chose PC: αTA: Kolliphor® HS15: R = 7:22:22:4 as the final formula for both Rnano and L-Rnano in this study.

Table S1. Nanoparticle characteristics

PC: αTA: Kolliphor® HS15: R (mg)	Particle size (nm)	PI	Encapsulation efficiency (%)	Comments
7:15:15:4	109.6 ± 0.3	0.18 ± 0.15	85.2	Low encapsulation efficiency
7:20:20:4	102.6 ± 0.2	0.21 ± 0.14	89.4	
7:22:22:4	92.0 ± 0.3	0.17 ± 0.01	92.0	High encapsulation efficiency
7:24:24:4	85.3 ± 0.2	0.18 ± 0.01	96.6	
7:30:30:5	102.5 ± 0.2	0.16 ± 0.04	95.3	No R precipitation after storing nanoparticles at 37°C for 24 hours
7:32:32:5	92.1 ± 0.3	0.18 ± 0.12	96.1	
7:34:34:5	85.3 ± 0.2	0.17 ± 0.11	97.4	
7:34:34:6	96.0 ± 0.3	0.17 ± 0.15	86.9	R precipitation after storing nanoparticles at 37°C for 24 hours
7:36:36:6	83.1 ± 0.1	0.12 ± 0.01	96.0	
7:40:40:7	106.6 ± 0.2	0.20 ± 0.02	95.2	
7:42:42:7	99.3 ± 0.2	0.10 ± 0.02	96.5	
7:44:44:8	88.6 ± 0.2	0.20 ± 0.15	90.4	
7:46:46:8	81.1 ± 0.3	0.20 ± 0.20	93.8	

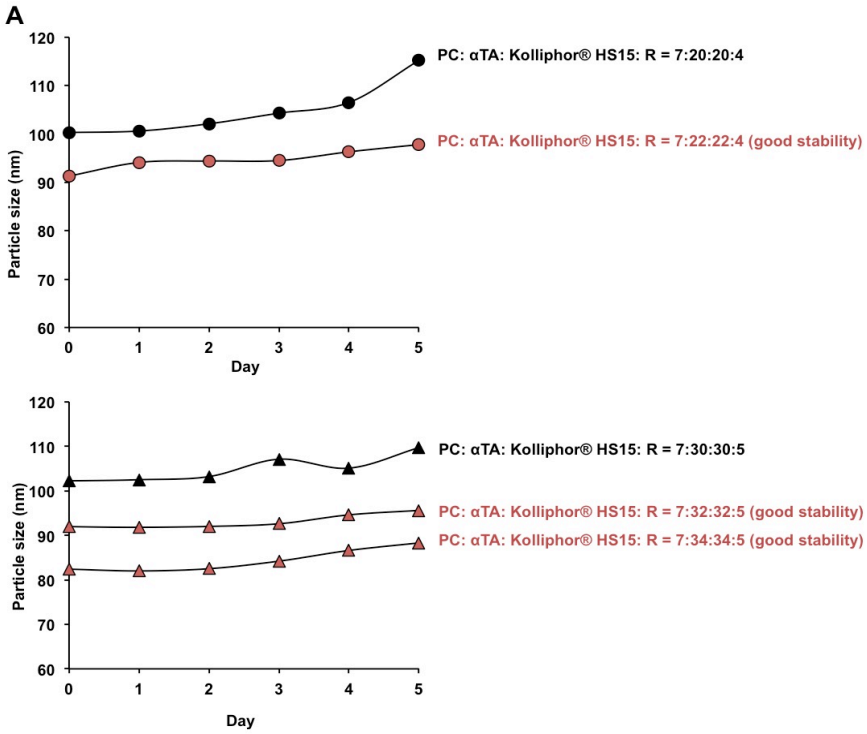
A
Particle size (nm)
Day
PC: αTA: Kolliphor® HS15: R = 7:20:20:4
PC: αTA: Kolliphor® HS15: R = 7:22:22:4 (good stability)
PC: αTA: Kolliphor® HS15: R = 7:30:30:5
PC: αTA: Kolliphor® HS15: R = 7:32:32:5 (good stability)
PC: αTA: Kolliphor® HS15: R = 7:34:34:5 (good stability)

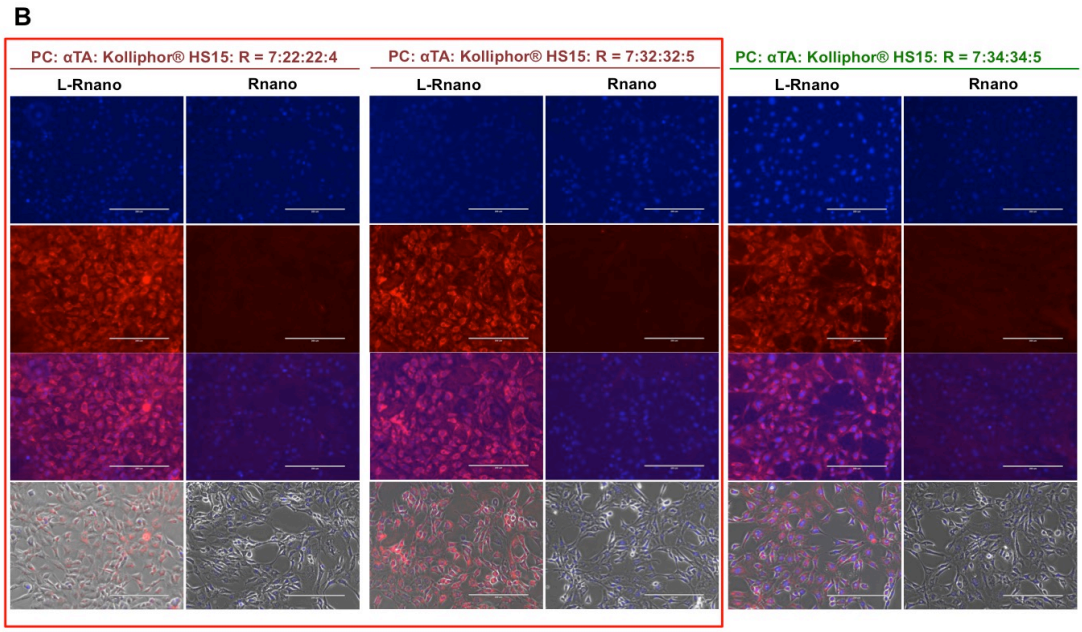
B
PC: αTA: Kolliphor® HS15: R = 7:22:22:4
PC: αTA: Kolliphor® HS15: R = 7:32:32:5
PC: αTA: Kolliphor® HS15: R = 7:34:34:5
L-Rnano
Rnano
L-Rnano
Rnano
L-Rnano
Rnano

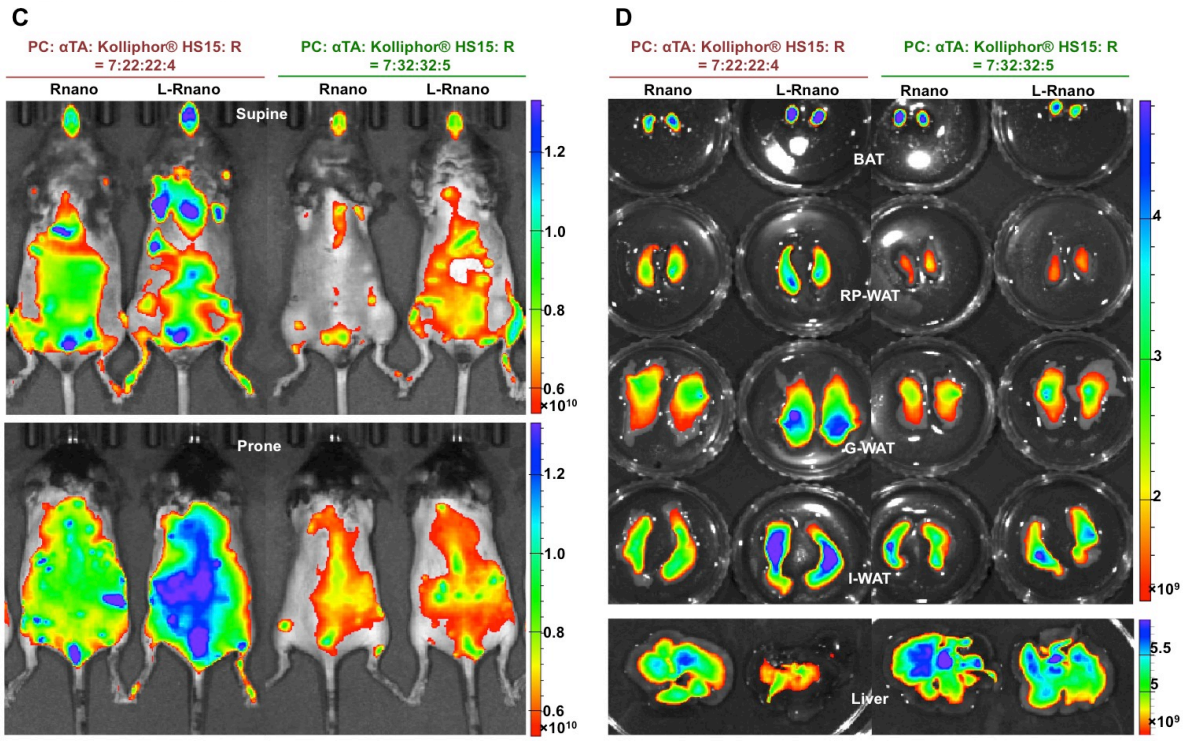

Fig. S1. Nanoparticle stability and binding affinity to ΔDCN cells *in vitro*, and target specificity and biodistribution *in vivo* during optimization of nanoparticle formulae. **(A)** Formulation screening based on the size and stability of nanoparticles. Rnano were prepared using different formulae and incubated at 37°C for 5 days. Particle size was measured using a Brookhaven BI-MAS particle size analyzer. **(B)** Formulation screening based on L-Rnano binding to and uptake by ΔDCN cells. Rhoda-labeled Rnano or L-Rnano (red) were prepared and incubated with ΔDCN cells for 2 hours at 37°C. Cells were fixed, stained with DAPI (blue) and imaged by a fluorescence microscope. Images are representatives of three independent experiments. Scale bar = 200 μm. **(C)** DiD-labeled Rnano or L-Rnano prepared using different formulae were injected intravenously into C57BL/6J mice. After 24 hours, DiD fluorescence was measured using the IVIS system on live mice. **(D)** DiD fluorescence was measured in isolated BAT, RP-WAT, GWAT, I-WAT, and liver. Radiance (p/s/cm^2/sr) is shown. Images are representative of three independent experiments.

2.2. Physical stability of Rnano and L-Rnano

The physical stability of Rnano and L-Rnano with the final formula in 1×PBS, as indicated by their particle size, PI and zeta potentials, was measured for 3 days at 4°C, 22°C, and 37°C. After 3 days, the average particle size of both Rnano and L-Rnano was increased by 22% at 4°C (refrigerator temperature), 40% at 22°C (room temperature), and 50% at 37°C (body temperature) (**Fig. S2**). Increased particle size with higher temperature may be related to the breakage of hydrogen bonds of Kolliphor® HS15, leading to reduced stability of Rnano and L-Rnano. PI of Rnano and L-Rnano was increased 22% and 20%, respectively, regardless of storage temperatures, indicating increased heterogeneity. After storage at all tested temperatures for 3 days, the absolute zeta potential of Rnano and L-Rnano was decreased by 30% and increased by 40%, respectively.

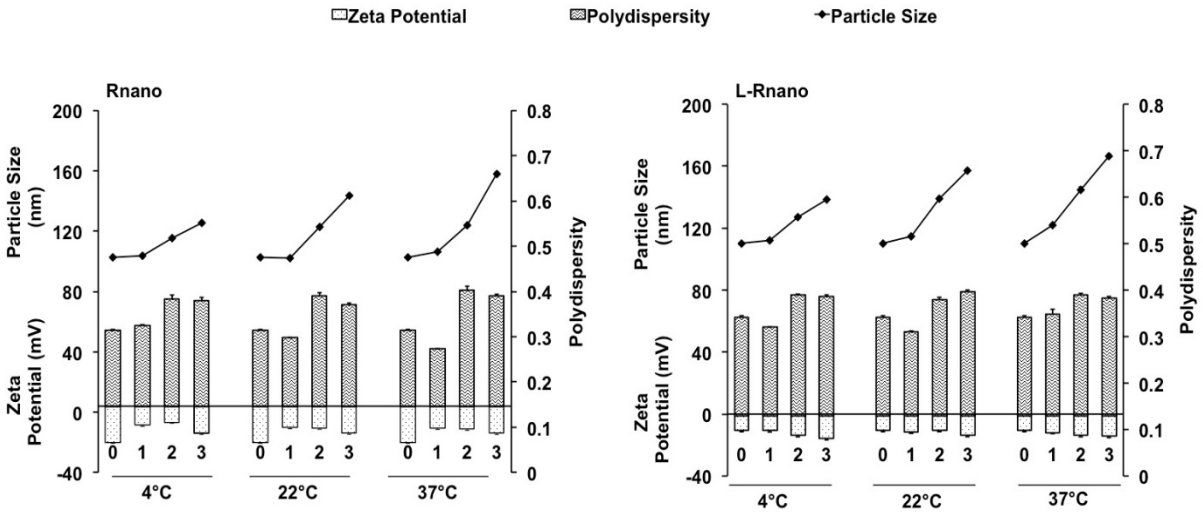

Fig. S2. Physical stability of Rnano and L-Rnano. Rnano and L-Rnano were incubated for 3 days at 4°C, 22°C, and 37°C. Changes in particle size, PI and zeta potential were measured by Brookhaven BI-MAS particle size and Zeta PALS analyzer.

2.3. DiD intensity of fat depots and the liver

After intravenous administration of DiD-labeled Rnano or L-Rnano to obese C57BL6J mice, the DiD intensity in different fat depots and liver were measured. Compared to Rnano, L-Rnano had 1.8-fold higher accumulation in I-WAT and 1.2-fold lower accumulation in the liver (**Fig. S3**). There were no significant differences in the fluorescence intensity in interscapular BAT (I-BAT) between Rnano and L-Rnano groups (**Fig. S3**).

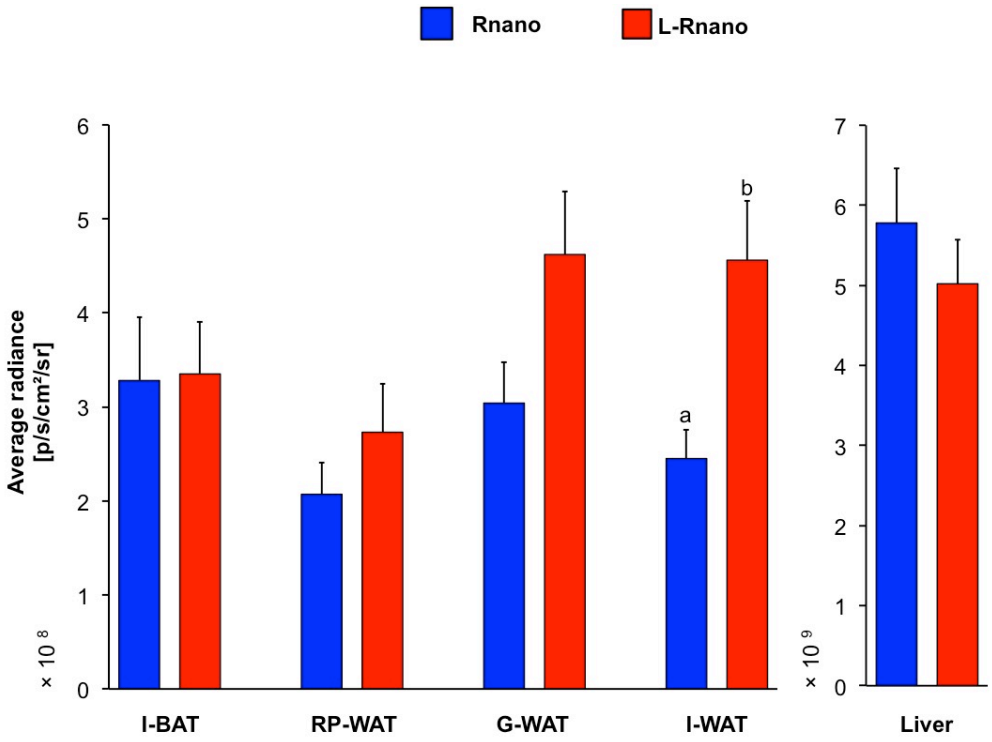

Fig. S3. Nanoparticle signals in the liver, BAT and different WAT depots of Rnano- and L-Rnano-treated mice. The IVIS data were quantitated for I-BAT, RP-WAT, G-WAT, I-WAT and liver isolated from DiD-labeled Rnano or L-Rnano-treated study mice. Data are expressed as mean ± SEM. Bars without a common superscript differ, $p<0.05$.

2.4. ASC target specificity of L-Rnano in RP-WAT.

After isolating SVF from RP-WAT, and identifying ASCs with antibodies, L-Rnano-treated mice had more “DiD+ ASCs” in RP-WAT (4.8-fold) than Rnano-treated mice, which were similar to the high “DiD+ ASCs” ratio in G-WAT and I-WAT of L-Rnano-treated mice (**Fig. S4**).

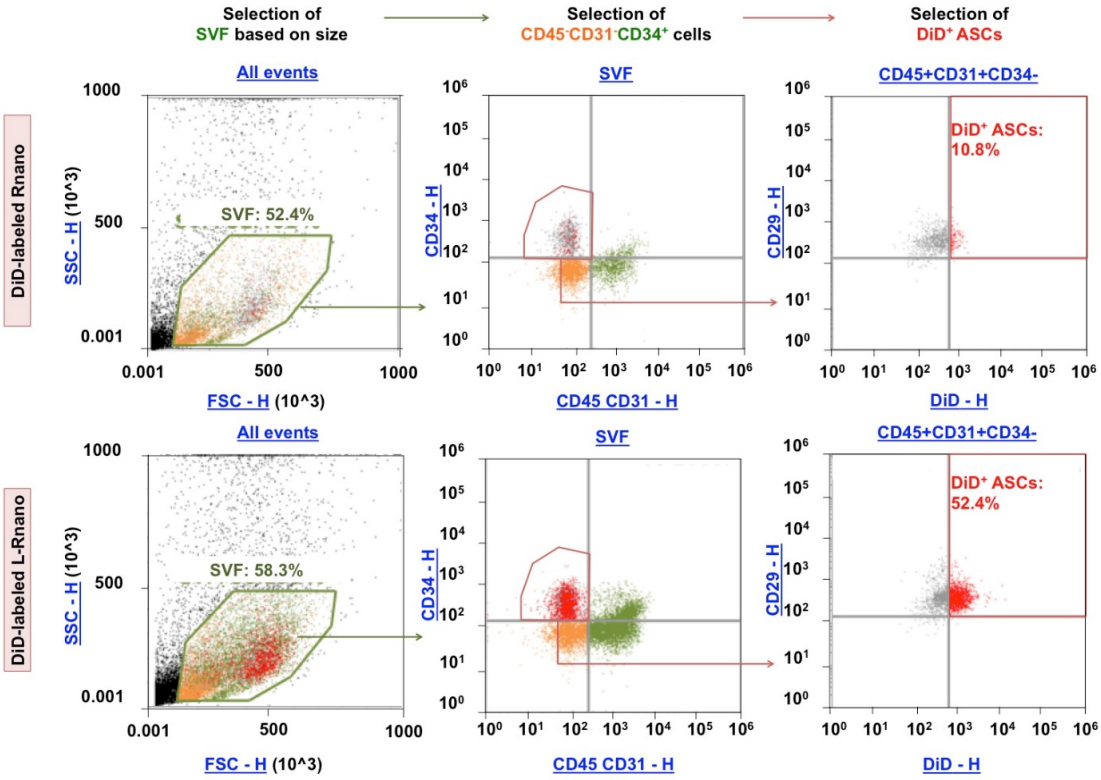

Fig. S4. ASC target specificity of L-Rnano in RP-WAT. After isolating SVF cells from RP-WAT from the study mice, the SVF cells were stained with antibodies, and ASCs were identified as $CD45^-/CD31^-/CD34^+/CD29^+$ by flow cytometry. Binding and uptake of DiD-labeled Rnano or L-Rnano by ASCs in RP-WAT were measured by flow cytometry.

2.5. Weights of the RP-WAT and I-BAT

Compared to free R-treated mice, Rnano-treated and L-Rnano-treated mice had 1.71- and 2.22-fold ($p<0.05$) lower RP-WAT mass, and 1.16- and 1.24-fold ($p<0.05$) lower I-BAT mass, respectively (**Fig. S5**).

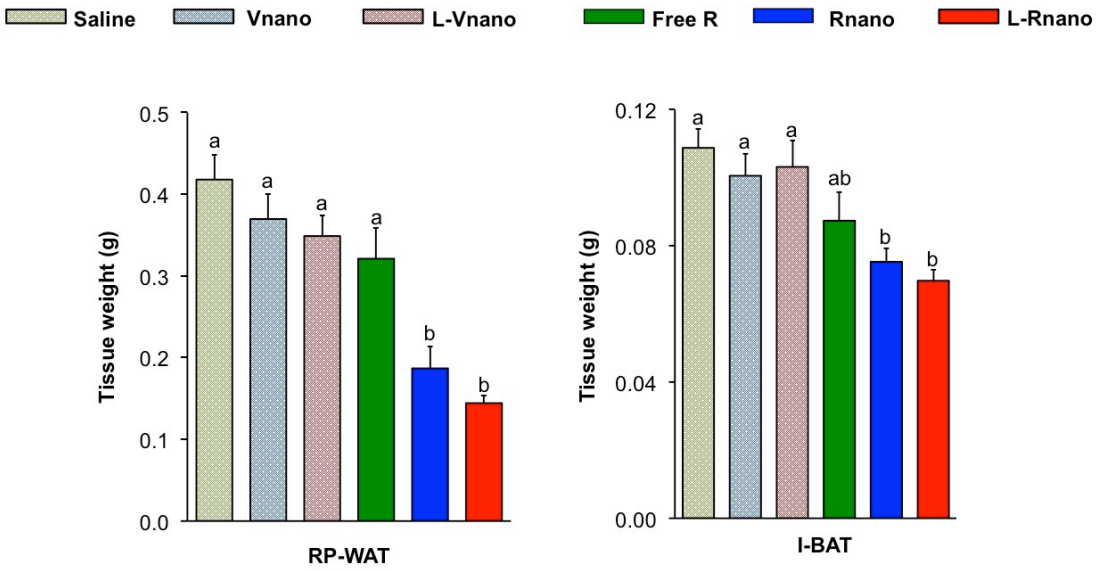

Fig. S5. RP-WAT and I-BAT masses. RP-WAT and I-BAT were isolated from the study mice and weighed by a microscale (n=10). Data are expressed as mean ± SEM. Bars without a common superscript differ, $p<0.05$.

2.6. Representative images of G-WAT and I-WAT

The appearance of G-WAT and I-WAT excised from mice is shown in **Fig. S6**. L-Rnano-treated mice had the smallest G-WAT and I-WAT among 6 groups, which correlated with the lowest body weight and % body fat.

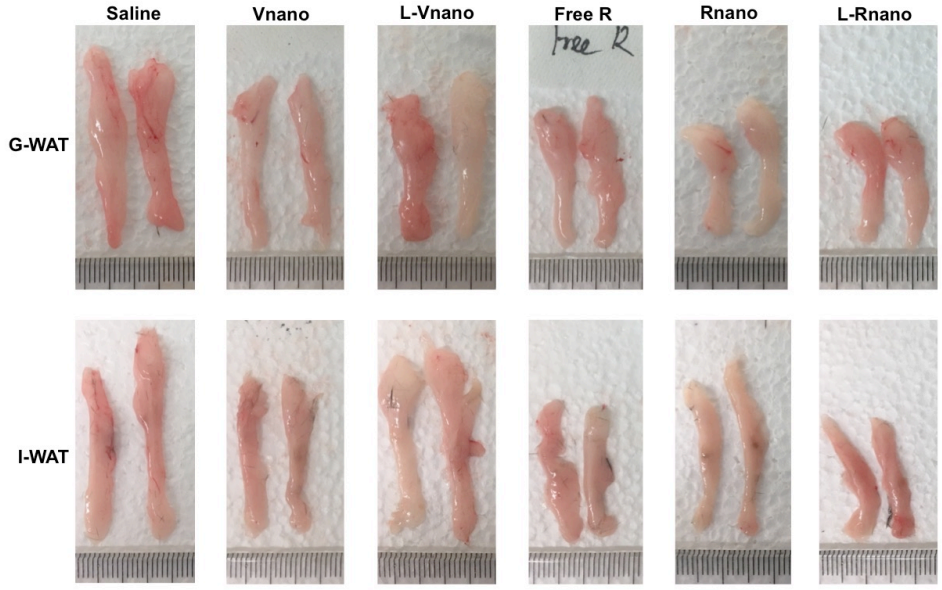

Fig. S6. Representative images of G-WAT and I-WAT. Comparison of the size of G-WAT and I-WAT excised from mice of each treatment.

2.7. I-WAT and G-WAT mRNA expression

The beige adipocyte selective marker CD137 mRNA levels in I-WAT of L-Rnano-treated mice were 2.65- and 1.56-fold ($p<0.05$) higher than that in mice treated with free R and Rnano, respectively (**Fig. S7A**). However, there were no significant differences in the mRNA levels of PGC-1α, PRDM16, PPAR-γ, and TMEM26 in I-WAT among all treatment groups (**Fig. S7A**). We also measured UCP-1 mRNA levels in G-WAT, UCP-1 mRNA levels in G-WAT isolated from Rnano-treated mice were 1.86- and 2.30-fold higher than that of the free R- and L-Rnano-treated mice, respectively (**Fig. S7B**).

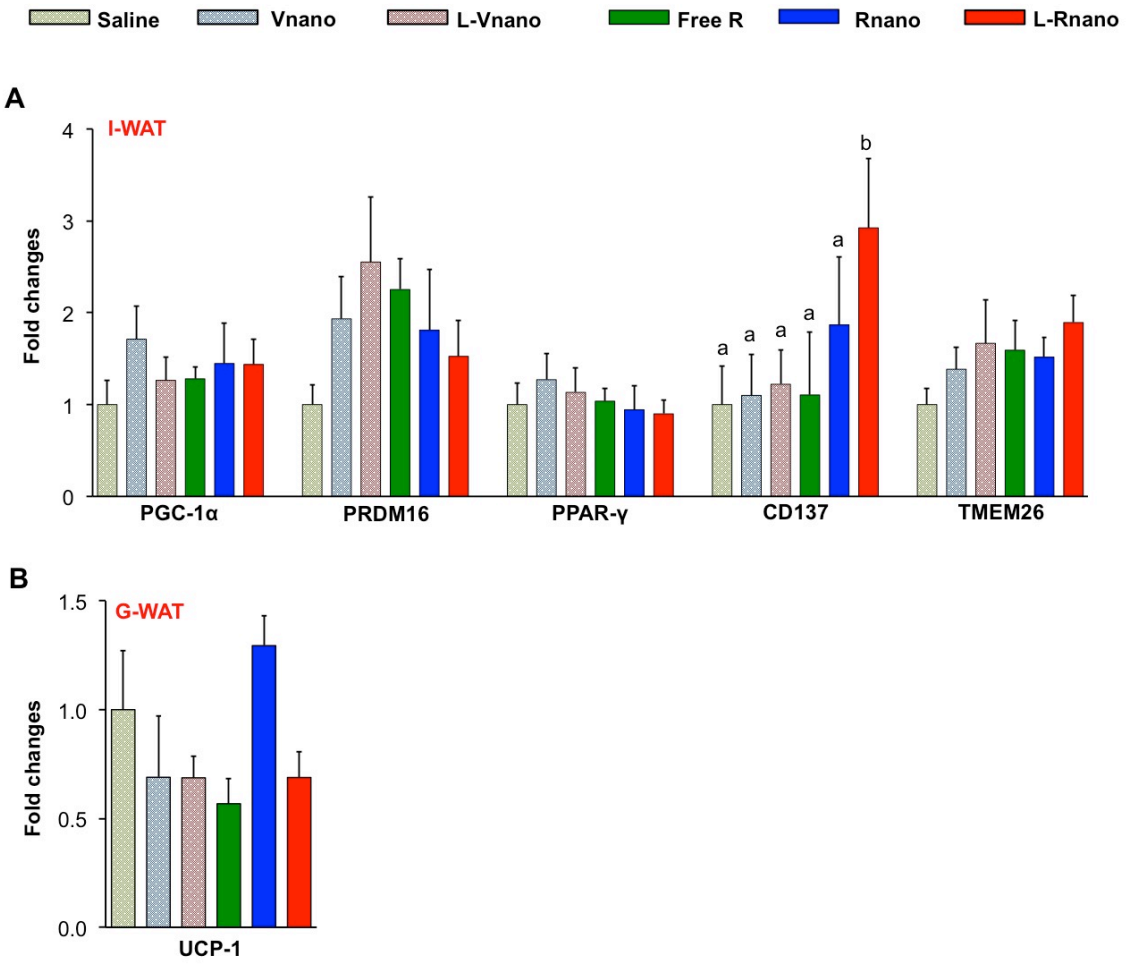

Fig. S7. Gene expression of browning markers in I-WAT and UCP-1 expression in G-WAT. **(A)** mRNA levels of PGC-1α, PRDM16, PPAR-γ, CD137 and TMEM26 in I-WAT were measured by real-time PCR (n=7). **(B)** mRNA levels of UCP-1 in G-WAT were measured by real-time PCR (n=7). Data are expressed as mean ± SEM. Bars without a common superscript differ, $p<0.05$.

2.8. Inflammatory cytokines expression

Plasma concentrations of inflammatory cytokines were measured in six treatment groups. Rnano-treated and L-Rnano-treated mice had the lowest plasma concentrations of TNFα, IL-6, IFNγ and MCP-1 among all groups of mice (**Fig. S8A**). This suppression could be accompanied by decreasing macrophage infiltration in I-WAT. Therefore, we measured the expression of F4/80, the macrophage-specific marker, in I-WAT and found that L-Rnano-treated mice had 2-fold lower F4/80 mRNA levels than that of free R-treated mice (**Fig. S8B**).

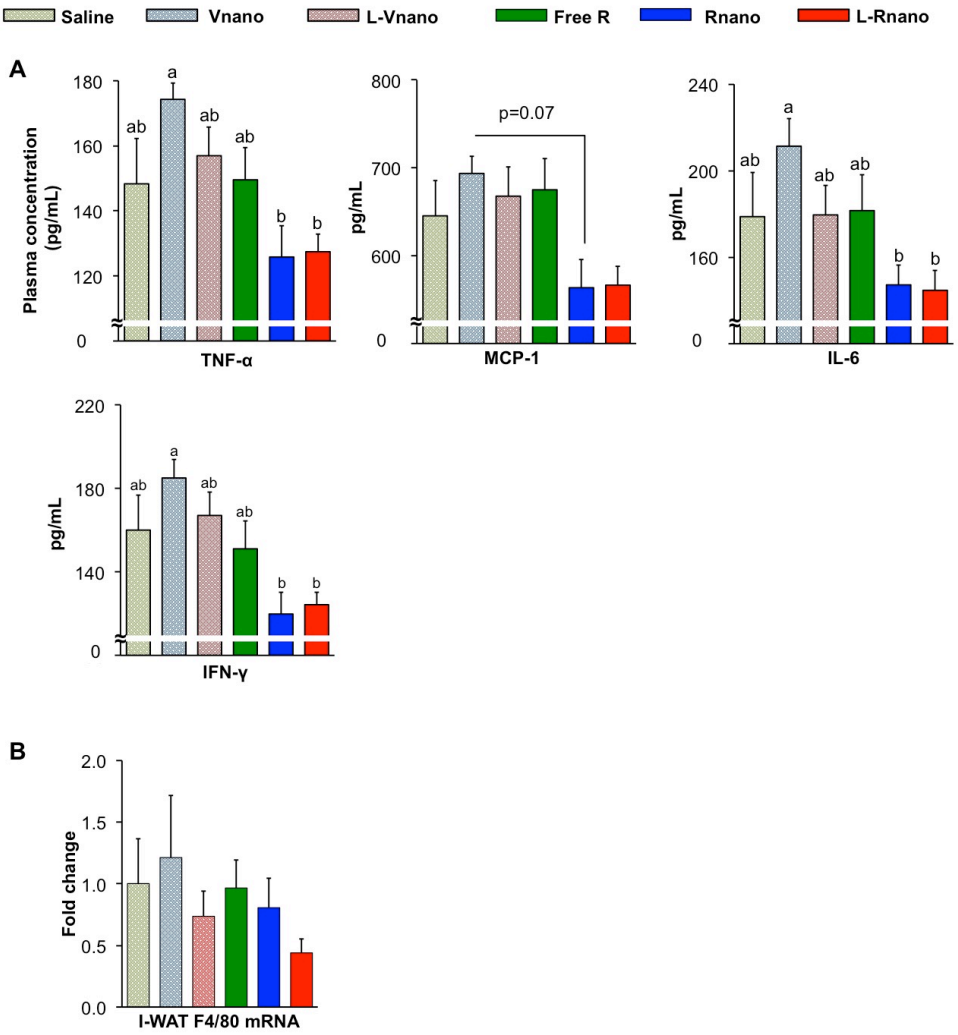

Fig. S8. Plasma concentrations of inflammatory factors and F4/80 gene expression in I-WAT. **(A)** Plasma concentrations of TNF-α, MCP-1, IL-6, and IFN-γ were measured by a BioLegend® LEGENDplex™ inflammation kit (n=7). **(B)** mRNA levels of F4/80 in I-WAT were measured by real-time PCR (n=7). Data are expressed as mean ± SEM. Bars without a common superscript differ, $p<0.05$.

2.9. Safety evaluation

Histological examinations of the liver, heart, lung, kidneys, brain, spleen, and skeletal muscle of study mice have been conducted we evaluate the safety of Rnano and L-Rnano. And no significant differences between the saline and the other treatments have been observed (**Fig. S9**).

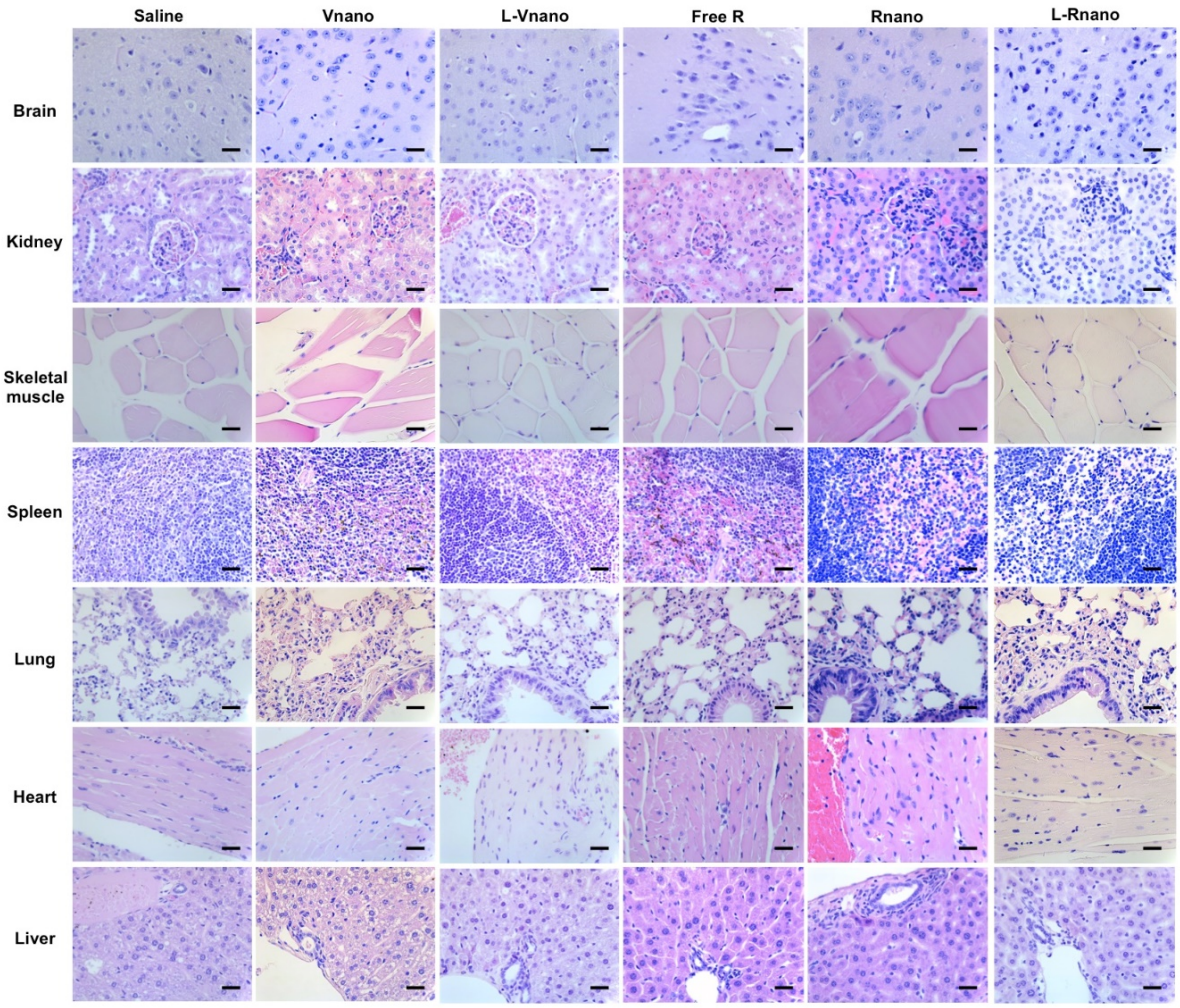

Fig. S9. Histological evaluation of tissues and organs. The representative H&E histological images of the heart, liver, lungs, kidneys, skeletal muscle, brain, and spleen from the study C57BL/6J mice, n=5. The tissue slides were fixed, embedded, sectioned, and stained for histological examination and evaluation, which were conducted by pathologists and scientists at Texas A&M Veterinary Medical Diagnostic Laboratory. Scale bar length is 50 μm.

Table S2. Serum chemistry panel

	Saline	Vnano	L-Vnano	Free R	Rnano	L-Rnano
Liver panel						
Total Bilirubin (mg/dL)	0.2 ± 0.1	0.2 ± 0.1	0.2 ± 0.1	0.2 ± 0.1	0.1 ± 0.1	0.2 ± 0.1
Aspartate amino transferase (U/L)	72.3 ± 4.3	76.4 ± 21.1	81.0 ± 12.5	79.4 ± 7.2	101.0 ± 14.9	77.7 ± 24.2
Alanine amino transferase (U/L)	23.3 ± 2.6	17.6 ± 2.1	19.0 ± 2.9	16.8 ± 0.7	20.8 ± 3.1	21.3 ± 5.8
Alkaline phosphatase (U/L)	48.5 ± 3.5	26.4 ± 9.1	26.5 ± 8.3	43.0 ± 9.7	22.5 ± 6.0	33.5 ± 9.7
Glutamate dehydrogenase (U/L)	20.0 ± 1.6	1.06 ± 2.2	22.8 ± 2.4	17.2 ± 1.0	22.7 ± 8.3	15.5 ± 2.5
Renal Panel						
Total Serum Protein (g/dL)	5.25 ± 0.1	5.02 ± 0.2	5.03 ± 0.1	5.06 ± 0.1	4.8 ± 0.2	5.1 ± 0.2
Albumin (g/dL)	3.2 ± 0.1	3.1 ± 0.1	2.9 ± 0.1	2.9 ± 0.1	2.8 ± 0.1	2.8 ± 0.1
Creatinine (mg/dL)	0.2	0.2	0.2	0.2	0.2	0.1
Blood urea nitrogen (BUN) (mg/dL)	25.8 ± 1.7	25.6 ± 1.0	26.3 ± 1.8	28.4 ± 0.9	28.0 ± 2.1	30.5 ± 1.7
Electrolytes						
Sodium (mEq/L)	150.7 ± 2.3	153.0 ± 3.3	151.0 ± 1.8	147.6 ± 3.2	149.5 ± 3.6	156.7 ± 4.0
Potassium (mEq/L)	9.0 ± 0.6	7.8 ± 0.2	8.2 ± 0.3	8.5 ± 0.4	7.5 ± 0.3	8.7 ± 0.4
Na/K Ratio	16.9 ± 1.0	19.4 ± 0.2	19.4 ± 1.0	19.4 ± 0.7	19.4 ± 0.4	19.4 ± 0.5
Chloride (mEq/L)	108.5 ± 1.9	103.0 ± 4.2	104.0 ± 2.1	105.6 ± 3.6	104.7 ± 2.8	114.2 ± 1.3
Calcium (mg/dL)	7.7 ± 1.4	6.2 ± 1.4	4.9 ± 0.9	6.7 ± 1.3	4.0 ± 0.0	7.6 ± 1.9
Others						
Albumin to globulin (A/G ratio)	1.6 ± 0.2	1.7 ± 0.1	1.4 ± 0.1	1.4 ± 0.1	1.3 ± 0.1	1.3 ± 0.1
Globulins (g/dL)	2.0 ± 0.1	1.9 ± 0.1	2.1 ± 0.1	2.2 ± 0.1	2.1 ± 0.1	2.2 ± 0.1
Amylase (U/L)	728.5 ± 7.8	997.4 ± 334.1	670.5 ± 52.0	723.0 ± 75.0	679.0 ± 85.6	571.0 ± 18.5

Table S3. Primer sequences

36B4	Forward	GCTTCGTGTTCACCAAGGAGGA
	Reverse	GTCCTAGACCAGTGTTCTGAGC
UCP-1	Forward	GCTTTGCCTCACTCAGGATTGG
	Reverse	CCAATGAACACTGCCACACCTC
PPARγ	Forward	GTACTGTCGGTTTCAGAAGTGCC
	Reverse	ATCTCCGCCAACAGCTTCTCCT
PGC-1α	Forward	GAATCAAGCCACTACAGACACCG
	Reverse	CATCCCTCTTGAGCCTTTCGTG
PRDM16	Forward	ATCCACAGCACGGTGAAGCCAT
	Reverse	ACATCTGCCCACAGTCCTTGCA
CD137	Forward	CGTGCAGAACTCCTGTGATAAC
	Reverse	GTCCACCTATGCTGGAGAAGG
Tmem26	Forward	ACCCTGTCATCCCACAGAG
	Reverse	TGTTTGGTGGAGTCCTAAGGTC
Leptin	Forward	TGGGGTTTTGGAGCAGTTTG
	Reverse	CTGTCACTCTTTCCCGGTCT